A HYDROCODE EOS FOR PYROLITIC MANTLES AND MAGMA OCEANS. S.T. Stewart[1], B.A. Chidester[2], R. Caracas[3], J. Badro[3], M.L. Harwell[1], M. Huff[4], S.B. Jacobsen[5], P. Kalita[6], D.K. Spaulding[1], [1]U. California Davis, [2]Los Alamos National Lab., [3] CNRS, IPGP, [4]U. Rochester, [5]Harvard U., [6]Sandia National Labs., (sts@ucdavis.edu).

Introduction: During terrestrial planet formation, radioactive heat and the energy of accretion produced magma oceans on the growing planets. Thus, the giant impact stage likely involved collisions between protoplanets with a range of thermal profiles, from fully molten mantles to fully solid mantles. It has been difficult to construct equation of state models for silicates over the wide range of pressures and temperature of planet formation. Silicate liquids in particular have rapid changes in compressibility associated with the evolving coordination structure and thermodynamic parameters [1, 2, 3, 4]. In addition, most shock wave data have been obtained on single minerals (e.g., forsterite, olivine, enstatite) whereas the bulk composition of rocky planets is comprised of several minerals that vary with depth.

Pyrolite is a compositional model for the chemistry and mineralogy of the bulk silicate Earth [5]. It is also representative of the composition of magma oceans on the proto-Earth and similar terrestrial planets. Here, we present new shock data on a synthetic pyrolitic glass and the development of a model equation of state for pyrolite with the widely-used Analytic Equations of State (ANEOS) code package [6]. The ANEOS code has been updated to have more flexiblity in fitting the thermodynamics of silicate liquids [4, 7]. As an illustration of the new ANEOS model, we revisit the canonical Moon-forming giant impact hypothesis, where a grazing Mars-sized body struck the proto-Earth. We investigate whether or not a canonical giant impact onto the proto-Earth has a different outcome with a solid mantle or a magma ocean.

Shock Experiments on Pyrolitic Glass: Pyrolitic glass beads were synthesized at IPGP using the laser levitation technique as described in [10]. There was some visible color variation within each sample, but negligible chemical variation across the samples as determined by electron microprobe analysis. The average density of the glass beads (2.94 ± 0.04 g/cm^3) was determined using an Archimedian balance.

Shock compression experiments were carried out at OMEGA EP, a laser-driven shock platform at the University of Rochester's Laboratory for Laser Energetics (LLE) and the Sandia Z Machine. Figure 1 presents the data from Omega EP. P-ρ (pressure-density) data between 290 and 1300 GPa and decaying shock T-U_S (temperature-shock velocity) data between 7200 and 60,000 K. A line-VISAR system provided time- and spatially-resolved shock velocity and optical reflectivity [11]. Optical emission was tracked using streaked optical pyrometry [12]. From the time-resolved record of the shock front spectral radiance in the decaying shock experiments, we can determine the shock temperature during shock transit through the sample. The quartz crystals served as a reflectivity and temperature standard. As in [9], having two quartz reference plates in our target assembly allowed us to correct for optical absorption in the pyrolite glass. In this case, the thermal emission of the shock wave was corrected for average absorption of light within the unshocked pyrolite by adjusting the optical depth of pyrolite iteratively until the reflectivity of both quartz crystals matched the expected reflectivity [13, 14].

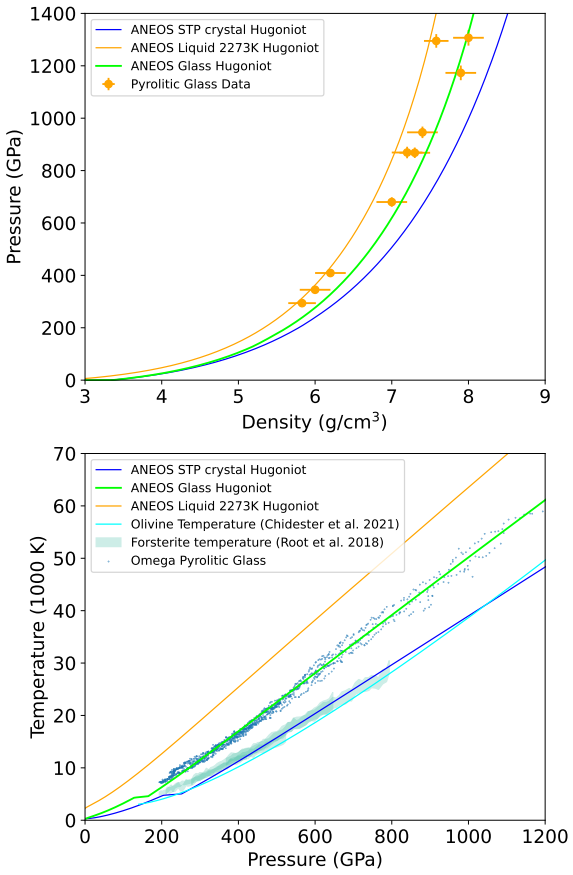

Figure 1: Shock Hugoniots for solid, glass, and liquid initial states from the new ANEOS model for pyrolite. New shock data on pyrolitic glass [this work] and shock temperature data on forsterite [8] and olivine [9].

A new ANEOS model for pyrolite: We fitted parameters for an ANEOS model with a simplified pyrolitic

composition ($Ca_{0.87}Fe_{2.03}Mg_{20.22}Al_{1.98}Si_{16.27}O_{58.63}$) (https://github.com/ststewart/aneos-pyrolite-2022). This model incorporates the data from our shock experiments on pyrolitic glass and ab initio calculations of the EOS of pyrolite along isotherms that intersect the liquid-vapor curve [15]. The model approximates pyrolite as a single component material with solid, liquid, vapor and ionization. As a result, the true solidus-liquidus region is not represented and the model melt curve is imposed near the peridotite solidus. In previous work, a pure forsterite model was often used to represent terrestrial mantles in hydrocode calculations [16]. The pyrolite model is preferred for a bulk mantle because of (1) more accurate shock temperatures in the liquid field with the addition of our glass data, (2) improved compressibility of liquid at lower pressures, and (3) improved volume change upon melting.

Moon-forming giant impact: Recently, [17] proposed that a canonical giant impact onto a proto-Earth with a magma ocean could emplace a larger fraction of proto-Earth material in the disk compared to an impact onto a solid proto-Earth. The observed isotopic similarity between the present-day Earth and Moon is a challenge for the canonical giant impact scenario, and a larger proportion of proto-Earth material in the lunar disk, or extensive mixing, is required to explain the observations. [17] used different equation of state models for the solid mantle and magma ocean, which raises the question of systematic differences in the prediction of the composition of the disk. We modeled the canonical Moon-forming giant impact using the GADGET2 smoothed particle hydrodynamics (SPH) code modified for planetary collisions (https://github.com/PhilJCarter/gadget2-planetary). We used the pyrolite ANEOS for the mantle and an iron-alloy ANEOS [18] for the core of each body. Using the new pyrolite multi-phase ANEOS, target bodies were initialized with a mantle that was fully solid or fully liquid in the upper mantle. We find that the material emplaced in the disk reached strong shock pressures, with about 70% (50%) of the mass experiencing pressures in excess of 50 GPa (85 GPa). The different initial thermal profiles produced similar projectile mass fractions in the disk (Fig. 2). The first contact of the graze-and-merge event transforms the proto-Earth into a super-critical body, so there is little difference in the outcome of the second contact with the projectile that provides the torque to emplace most of the material into the disk. For the canonical Moon-forming giant impact scenario, our results indicate that the initial thermal state of the proto-Earth was not a strong influence on the proportion of projectile material emplaced in the lunar accretion disk.

Acknowledgments: This work was supported by NSF PHY-2020249, SSAA DE-NA0003904, and the Sandia Z Fundamental Science Program (ZFSP). Sandia National Labs is managed and operated by National Technology and Engineering Solutions of Sandia, LLC., for the DOE-NNSA under contract DE-NA0003525; Sandia contribution SAND2022-0266 A. RC acknowledges support from ERC grant 681818 and access to supercomputing facilities via eDARI stl2816 and PRACE RA4947 grants. We thank Marcus Knudson and Heath Hanshaw for their support of the ZFSP experiments.

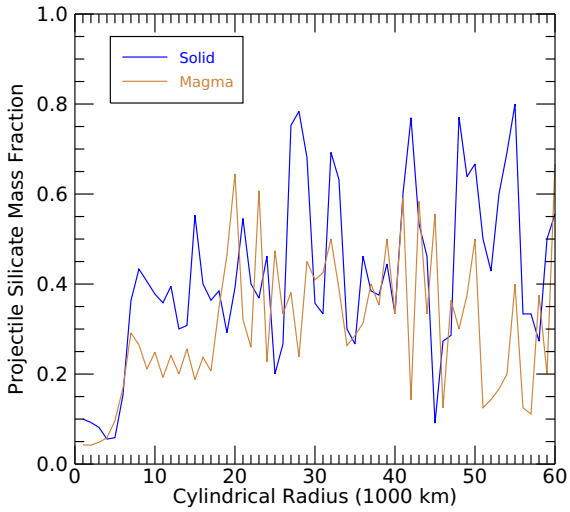

Figure 2: Distribution of projectile material at 24 hours after a canonical giant impact onto a proto-Earth with a solid mantle (blue) and magma ocean (brown).

References: [1] Jing Z. and Karato S.-i. (2011) *GCA*, *75*, 6780. [2] Asimow P. D. (2018) *Magmas Under Pressure*, 387. [3] Davies E. J. et al. (2020) *JGR Planets*, *125*, 1. [4] Stewart S. et al. (2020) *AIP Conf. Proc. SCCM19*, 080003. [5] McDonough W. and Sun S.-s. (1995) *Chemical Geology*, *120*, 223. [6] Thompson S. L., Technical Report Sandia SC-RR-70-28 (1970). [7] Thompson S. L. et al., M-ANEOS v1.0, Zenodo (2019), 10.5281/zenodo.3509365. [8] Root S. et al. (2018) *GRL*, *45*, 3865. [9] Chidester B. A. et al. (2021) *GRL*, *48*, e2021GL092471. [10] Badro J. et al. (2021) *Comptes Rendus. Géoscience*, *353*, 101. [11] Celliers P. M. et al. (2004) *RSI*, *75*, 4916. [12] Gregor M. C. et al. (2016) *RSI*, *87*. [13] Hicks D. G. et al. (2006) *PRL*, *97*, 3. [14] Millot M. et al. (2015) *Science*, *347*, 418. [15] Caracas R. and Stewart S. T. (2022) *LPSC 53*, 1630. [16] Stewart S. et al., Zenodo (2019), 10.5281/zenodo.3478631. [17] Hosono N. et al. (2019) *Nature Geo.*, *12*, 418. [18] Stewart S. T. (2020), *Zenodo*, 10.5281/zenodo.3866550.